

SURVEYS OF GALAXY CLUSTERS WITH THE SUNYAEV-ZEL'DOVICH EFFECT

A. E. SCHULZ¹ AND MARTIN WHITE²

Received 2002 October 30; accepted 2002 December 6

ABSTRACT

We have created mock Sunyaev-Zel'dovich effect (SZE) surveys of galaxy clusters using high-resolution N -body simulations. To the pure surveys, we add “noise” contributions appropriate to instrument and primary cosmic microwave background anisotropies. Applying various cluster finding strategies to these mock surveys, we generate catalogs that can be compared to the known positions and masses of the clusters in the simulations. We thus show that the completeness and efficiency that can be achieved depend strongly on the frequency coverage, noise, and beam characteristics of the instruments, as well as on the candidate threshold. We study the effects of matched filtering techniques on completeness and bias. We suggest a gentler filtering method than matched filtering in single-frequency analyses. We summarize the complications that arise when analyzing the SZE signal at a single frequency and assess the limitations of such an analysis. Our results suggest that some sophistication is required when searching for “clusters” within an SZE map.

Subject headings: cosmology: theory — galaxies: clusters: general

1. INTRODUCTION

Observations of the number density of clusters of galaxies will play an increasingly important role in determining the composition of the energy density in the universe as data from the myriad of upcoming cluster surveys accumulate. Cluster surveys result in constraints orthogonal in parameter space to those obtained from other cosmological observations, such as the cosmic microwave background (CMB) anisotropies and supernova searches, because the cluster abundance depends significantly on the linear growth function. For this reason, clusters can also be used to probe the nature and evolution of the dark energy in the universe. Since clusters are the most recently formed gravitationally bound objects in the universe, the evolution of their number density sensitively probes the critical redshift range $0 < z < 2$, a range over which the dark energy has come to dominate the total energy density. Clusters are convenient in that they are very bright and rare enough to make counting them tractable.

A wide array of survey techniques is being used to conduct searches for clusters, making use of optical and X-ray emissions from clusters, weak lensing distortions, and the Sunyaev-Zel'dovich effect (SZE; see Table 1). The SZE is a particularly promising approach for finding galaxy clusters because the signal is relatively independent of the cluster's distance from us. This implies that, at least in principle, the selection function for such surveys is very well known. This is crucial if we are to use the cluster catalogs to measure the evolution of the number density of clusters.

Using the SZE does present certain difficulties. The energy lost by the CMB photons on their journey from the last scattering surface is an integrated effect. Hence, the SZE signal suffers from projection effects from other objects in the same line of sight as the cluster and also yields no information about the redshift of the cluster, save its angular size on the sky. Thus, to study evolution effects in the number

density, a follow-up observation is required to obtain the redshifts and, in rare cases, to distinguish between two separate clusters that lie in the same line of sight. The primary CMB anisotropies are also a problem, having significant power on cluster-sized angular scales. Finally, since clusters of galaxies are not perfect, isolated spheres of gas, the SZE signal obtained from a cluster of a given mass will vary considerably depending on the particular line of sight through the cluster. These effects make it difficult to correlate the SZE signal with the actual mass of the cluster causing it. In this paper we make a preliminary investigation of the power of SZE surveys in finding clusters, taking these effects into account, and present the results in terms of the completeness and efficiency of mass-limited samples achievable using the SZE.

2. METHOD

We construct maps of the SZE effect at various frequencies using as input a high-resolution N -body simulation of structure formation in a Λ CDM cosmology. In this way, our method is similar to that of Kay, Liddle, & Thomas (2001). We make mock observations of these maps by adding signal from the primary CMB anisotropies to the SZE maps, convolving with a beam window function, and adding Gaussian random noise such as might be produced by the electronics in a real observation. We identify every cluster candidate in these mock observations using a specified method and check it against the true three-dimensional positions of the clusters in the same simulation.

We present our results in terms of the completeness and efficiency of the method in finding clusters above a mass threshold. Completeness is the ratio of the number of clusters we found using the mock SZE observation to the total number of massive clusters in the field of view. Out of the total number of cluster candidates that we identify in our SZE maps, only some of them will actually be clusters with a mass above the threshold of interest. Efficiency will measure the ratio of clusters found to the total number of candidates and is a measure of the amount of contamination suffered when using the SZE technique. The survey

¹ Department of Physics, Harvard University, Cambridge, MA 02138.

² Departments of Physics and Astronomy, University of California, Berkeley, CA 94720.

TABLE 1
SOME UPCOMING SUNYAEV-ZEL'DOVICH EXPERIMENTS

Name	Type	Frequency (GHz)	Resolution
Acbar ^a	Bolo	150–270	4
Bolocam ^b	Bolo	145	1
CBI ^c	HEMT	30	4.5
SZA ^d	HEMT	30	~1
AMI ^e	HEMT	15	~1
Amiba ^f	HEMT	30	~1
APEX ^g	Bolo	150	0.75
SPT ^h	Bolo	150	1
Planck ⁱ	Bolo	30–850	5

NOTE.—Type indicates the nature of the receivers, high electron mobility transistors (HEMTs), or bolometers. The frequency is given in GHz. The resolution is an estimate of the beam size, in arcminutes, and for the interferometers, this estimate is quite approximate. The last six experiments intend to undertake blank-field SZ surveys.

^a Additional information on Acbar can be found at <http://cosmology.berkeley.edu/group/swlh/acbar/>.

^b Additional information on Bolocam can be found at http://www.astro.caltech.edu/~lgg/bolocam_front.htm.

^c Additional information on CBI can be found at <http://www.astro.caltech.edu/~tjp/CBI/>.

^d Additional information on SZA can be found at <http://astro.uchicago.edu/SZE/>.

^e Additional information on AMI can be found at <http://www.mrao.cam.ac.uk/telescopes/ami/>.

^f Additional information on Amiba can be found at <http://www.asiaa.sinica.edu.tw/amiba/>.

^g Additional information on APEX can be found at <http://bolo.berkeley.edu/apexsz/>.

^h Additional information on SPT can be found at <http://astro.uchicago.edu/spt/>.

ⁱ Additional information on Planck can be found at <http://astro.estec.esa.nl/Planck/>.

efficiency will be important in planning follow-up observations with other instruments. Obviously, an SZE survey will be useful for many things besides creating an effectively mass-selected sample, but it is such a sample that is the easiest to compare with theories of structure formation. It has also become commonplace to describe SZE surveys as “effectively mass-limited,” and it is for these reasons that we focus on this metric here.

2.1. The N -Body Simulation

The starting point for constructing the maps is an accurate model of the spatial distribution of mass along the past light cone. We obtain this from an N -body simulation of 512^3 particles in a (periodic) cube of side $300 h^{-1}$ Mpc run with a TreePM-SPH code (see the appendix of White 2002). Since on the scales of relevance to us baryonic pressure is subdominant, only collisionless dark matter is modeled, allowing us to achieve a higher dynamic range in the simulation. This allows us to simulate a larger volume, containing more of the rare rich clusters we are interested in, at the expense of an ad hoc (but flexible) treatment of the baryonic physics. The simulation is started at $z = 60$ and evolved to the present with the full phase space distribution dumped every $100 h^{-1}$ Mpc between redshifts $2 > z > 0$. It is this range of redshifts that dominates the SZE signal on the angular scales of interest to us, but by cutting off the integration at $z = 2$, we will underestimate the effect of confusion in our maps. The gravitational softening used is of a spline

form, with a “Plummer-equivalent” (comoving) softening length of $20 h^{-1}$ kpc. We have used a flat cosmology compatible with a host of current observations: $\Omega_m = 0.3$, $\Omega_\Lambda = 0.7$, $\Omega_b h^2 = 0.02$, $h = 0.7$, $n = 1$, and $\sigma_8 = 1$. The transfer function was evaluated with the fitting function of Eisenstein & Hu (1999). While a slightly lower σ_8 would better fit the inferred mass function of rich clusters from X-ray surveys, the higher σ_8 provides an easier match to the Cosmic Background Imager (CBI) deep-field observations (Mason et al. 2002). The mass resolution in the simulation is fine enough to identify galactic mass halos, with noninteracting dark matter particles of mass $1.7 \times 10^{10} h^{-1} M_\odot$. All of the relevant cluster-scale halos contain several thousand particles to begin to resolve the substructure. The simulation was performed on 128 processors of the IBM-SP2 at NERSC and took nearly 4000 time steps and approximately 100 wall clock hours to complete.

To construct the long thin line of sight used to compute the net SZE, we have stacked the intermediate stages of the simulation between redshifts $2 > z > 0$. In order to avoid multiply sampling the same large-scale structures, each $300 h^{-1}$ Mpc box has been randomly reoriented in one of the six possible orientations and has furthermore been shifted by a random amount, perpendicular to the line of sight, making use of the periodic boundary conditions. There are three time dumps per box length. Each $300 h^{-1}$ Mpc volume in the stack is made up of three segments, each segment evolved to a later epoch than the previous one by the time it takes light to travel $100 h^{-1}$ Mpc. We have chosen $100 h^{-1}$ Mpc as the sampling interval because it is large enough so that edge effects are minimal, yet fine enough that the line-of-sight integrals are well approximated by sums of the (static) outputs. Because of the periodicity, we are free to choose any of the thirds as the oldest, cyclically permuting the other two. This approach preserves the continuity of large-scale structure over distances of $300 h^{-1}$ Mpc without compromising the resolution in time evolution.

2.2. Cluster Catalog

In order to compute the completeness and efficiency with which the mock SZE survey can detect clusters, we need to know the true distribution of clusters in the simulated fields. To this end we construct a catalog of the three-dimensional position, redshift, mass, velocity dispersion, and other useful quantities of each identified halo above $10^{13} h^{-1} M_\odot$. Halos are identified using a friends-of-friends (FoF) algorithm (Davis et al. 1985) on each of the time dumps used in the line-of-sight integral. The FoF algorithm partitions the particles into equivalence classes by linking together all particle pairs separated by less than a distance b . We use a linking length of $b = 0.15$ times the mean interparticle spacing, which is smaller than the typical value of $b = 0.2$ because it reduces the number of instances in which two separate halos, connected by a filament of significant overdensity, get accidentally classified as a single object. Such misclassifications were found to be a significant source of confusion when computing completeness and efficiency (see also White & Kochanek 2002; Kochanek et al. 2003; White, van Waerbeke, & Mackey 2002 for further discussion). While the spherical overdensity algorithm, which is less susceptible to the merging problem, could have been used, this algorithm identifies spherical clusters that would

introduce a different type of bias. We use position of the potential minimum of the FoF group as the center of the cluster because it is more robust than using the center of mass, coinciding closely with the density maximum of the cluster for all but the most anomalous clusters. Centering on the potential minimum, we computed, for each halo, the mass, M_{200} , enclosed within a radius, r_{200} , interior to which the density contrast was 200 times the critical density. There are 6887 halos in the $z = 0$ three-dimensional catalog with $M_{200} > 10^{13} h^{-1} M_{\odot}$, of which 790 are more massive than $10^{14} h^{-1} M_{\odot}$ and nine have masses greater than $10^{15} h^{-1} M_{\odot}$. A typical simulated field will contain 200 or 300 halos more massive than $10^{14} h^{-1} M_{\odot}$.

2.3. Compton- y Maps

Because the simulation contains no gas, we use a semianalytic model to include the gas physics. First, we assume that the gas closely traces the dark matter. This is likely a good approximation in all regions except the innermost $O(100)$ kpc of the cluster, which for clusters at cosmological distances will be unresolved by the experiments of interest. (For an $\Omega_m = 0.3$ flat cosmology, 100 kpc subtends only $0'.26$ at $z = 0.5$, while upcoming survey experiments have beams of $\sim 1'$.) We ignore the presence of cold gas and stars in the intracluster medium, assuming that the mass in hot gas is Ω_b/Ω_m of the total. Second, each cluster is assumed to be isothermal. Our assumptions so far are similar to those of Cooray, Hu, & Tegmark (2000), but they additionally assumed that all of the gas in the universe was at fixed temperature, independent of the mass and virial temperature of the halo in which it resided. Instead, we assign to each particle in a group a temperature

$$\frac{k_B T}{\text{keV}} = T_* \left(\frac{M}{10^{15} h^{-1} M_{\odot}} \right)^{2/3} (\Delta_c E^2)^{1/3}, \quad (1)$$

where $E(z) \equiv H(z)/H_0$, Δ_c is the density threshold defining the mass and T_* gives the overall normalization of the relation. In principle, one could use a less steep function for lower masses, since there is some evidence that the T - M relation becomes shallower at low mass (Finoguenov, Reiprich, & Bohringer 2001). However, we also expect the gas fraction to drop to lower masses, and hydrodynamic simulations indicate that we can roughly mimic the effect of this on our SZE maps by keeping the slope of equation (1) fixed and holding f_{gas} at its universal value. Finally, we smoothly take $T \rightarrow 0$ for halo masses below $10^{13} h^{-1} M_{\odot}$. How we do this does not influence the results. Since most of the SZ emission comes from gas at significant overdensities (da Silva et al. 2001; White, Hernquist, & Springel 2002), considering only the particles in the halos when making the maps is a good approximation.

We use $T_* \sim 1$ throughout,³ which gives good agreement for the redshift evolution of the mean mass-weighted temperature and the angular power spectrum of y when compared with the results of hydrodynamic simulations (White et al. 2002). In particular, this method provides a better fit to the shape of the simulation based angular power spec-

³ For a power-law spectrum, $P(k) \sim k^n$, the SZE angular power spectrum scales as $T_*^2 \sigma_8^{14/(3+n)}$. Matching the local temperature function of rich clusters requires $\sigma_8 \sim T_*^{-\gamma}$ with $\gamma \simeq 0.7-0.9$. Thus, increasing T_* much above 1 drastically lowers the predicted SZE fluctuations if one maintains agreement with the observed X-ray temperature function.

trum, especially over the peak, than semianalytic methods (Komatsu & Kitayama 1999; Cooray 2000; Molnar & Birkinshaw 2000; Holder & Carlstrom 2001; Komatsu & Seljak 2002). As our approach has isothermal clusters, with a deterministic temperature derived solely from the mass, this somewhat limits the possible sources of discrepancy between the semianalytic and hydrodynamic calculations. There is a tendency for the N -body results to slightly underpredict (by tens of percent) the low- ℓ tail and to have less low-level unresolved emission than the hydro-based maps. Since the low- ℓ tail is sensitive to the volume used in constructing the maps and the hydro simulations were run in smaller boxes, we do not regard this disagreement as significant.

We choose T_* so that the power is close to the level seen by CBI in their deep field (Mason et al. 2002). This is a factor of approximately 4 larger than would be predicted by the ‘‘concordance’’ cosmology. Our results are relatively insensitive to the precise value of T_* chosen or to the treatment of ‘‘gas’’ outside of the virialized regions of halos. We generate Compton- y maps by integrating for each pixel

$$y = \int \sigma_T n_e \frac{k_B T_e}{m_e c^2} dl. \quad (2)$$

Here, σ_T is the Thompson scattering cross section and n_e , m_e , and T_e are the electron number density, mass, and temperature, respectively. We assume that within the clusters the gas is fully ionized. The contribution from each particle is distributed over the pixels with a spline weighting and a (physical) size equal to the smoothing length of the simulation. The temperature fluctuation at frequency ν is then obtained from the y -maps by

$$\frac{\Delta T}{T} = y \left(x \frac{e^x + 1}{e^x - 1} - 4 \right) \quad (3)$$

$$\simeq -2y \quad \text{for } x \ll 1, \quad (4)$$

where $x = h\nu/k_B T_{\text{CMB}} \simeq \nu/56.84$ GHz is the dimensionless frequency and the second expression is valid in the Rayleigh-Jeans limit. In what follows, we shall assume the low-frequency limit unless otherwise stated.

While these assumptions are crude, comparison of the maps with those made from the more sophisticated hydrodynamic simulations of White et al. (2002) shows that they capture many of the features of the more detailed modeling. The signals of interest are dominated by group- and cluster-sized halos that are quite regular in their gas properties, allowing a relatively simple-minded treatment for our purposes. It is important to note that since we are trying to *test* rather than *calibrate* our cluster extraction methods, our requirements on the simulated maps are not too stringent.

We generate 10 random SZE maps, each $3^\circ \times 3^\circ$ with 1024^2 pixels. An example map produced in this manner is shown in Figure 1. The map is clearly dominated by discrete sources, the galaxy clusters and rich groups, having a typical size of about $1'$ and a typical amplitude on the order of mJy.

2.4. Primary Cosmic Microwave Background Anisotropies

The primary CMB anisotropies contribute significantly to the SZE signal on the scales of interest to us, and it is important to consider the effects of contamination introduced by such fluctuations unless we can use multifrequency information to suppress the primary anisotropies. To

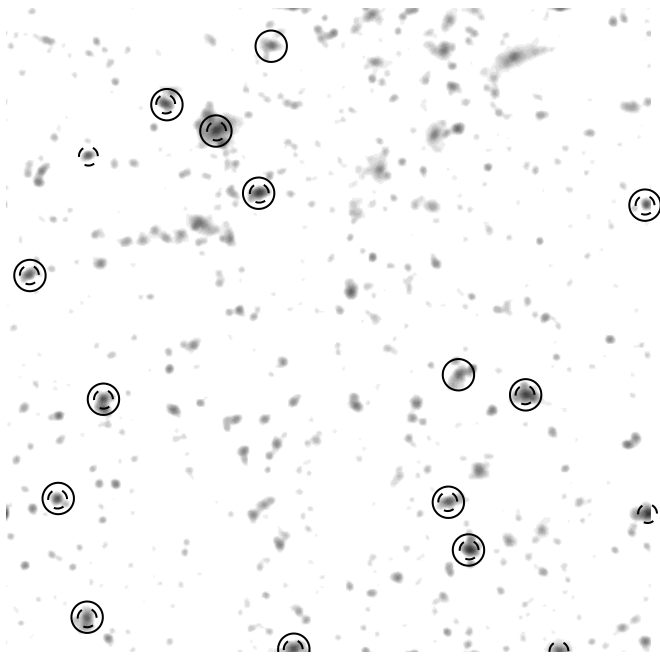


FIG. 1.—One SZE map, smoothed with a Gaussian of $1'$ FWHM but with *no noise added*. The gray scale is logarithmic, running from $10^{-5.5}$ to $10^{-3.5}$. There are 14 halos more massive than $4 \times 10^{14} h^{-1} M_{\odot}$ in the $3^{\circ} \times 3^{\circ}$ field (*solid circles*), of which 12 are found. There are 15 peaks above a threshold $y_{\text{cut}} = 5 \times 10^{-5}$ (*dashed circles*).

investigate this, we generate a large CMB map from which we extract a region of the same size as the SZE map and add it in as “noise.” We have used the CMBfast code to generate the CMB power spectrum for our cosmology (Seljak & Zaldarriaga 1996). The CMB map is then a random realization of a Gaussian field with this power spectrum. We generate random phases in momentum space and assign amplitudes to each of the k -modes using a distribution whose average value is the amplitude in the CMB power spectrum. We have used the flat-sky approximation, in which the k -mode in momentum space corresponds to ℓ value in the CMB power spectrum. The probability distribution function for the amplitudes, ρ , of each k -mode is given by

$$P(\rho^2) = \frac{1}{C_{\ell}} e^{-\rho^2/C_{\ell}}. \quad (5)$$

Thus, if ϵ is a random number between 0 and 1, ρ^2 will be given by

$$\rho^2 = -C_{\ell} \ln(\epsilon). \quad (6)$$

2.5. Matched Filter

After adding the CMB into the map, we convolve with a Gaussian beam, which smears the signal and obscures and information on scales much smaller than the beam size. To complete the mock observation, we add a few μK of white noise to each pixel corresponding to expected levels of noise from the electronics used in real observations. This introduces fluctuations on scales much smaller than the size of the features in the beam-smearred map.

In order to remove the CMB anisotropies and smooth the small-scale noise, it is necessary to filter the map; we exam-

ine a matched filter algorithm to optimize the contrast of signal to noise. The specific filter is described in (Tegmark & de Oliviera-Costa 1998, eq. [6]; see also Haehnelt & Tegmark 1996). It is azimuthally symmetric and has a radial dependence in Fourier space of

$$W_{\ell} \propto \frac{1}{B_{\ell} C_{\ell}^{\text{TOT}}}. \quad (7)$$

Here, $B_{\ell} = e^{-\theta^2 \ell(\ell+1)/2}$ and C_{ℓ}^{TOT} refers to the sum of the power spectra of elements to be removed from the map, in our case the CMB and white noise. The noise power spectrum is given by $C_{\ell}^N = (\sigma_{\text{pix}} \theta_{\text{pix}})^{-2} B_{\ell}^{-2}$ (e.g., Tegmark & Efstathiou 1996). For the normalization of the filter, we use the 1σ value of the noise (only) map after it has been filtered with $W_{\ell} = 1/B_{\ell} C_{\ell}^{\text{TOT}}$. In this way, we can compare mock observations with different beam sizes and levels of noise in terms of the statistical significance of the cluster SZE signal above the white noise in the map. Note that in some cases, the instrumental noise level will be significantly below the “noise” induced from CMB anisotropies, so amplitudes in these maps can be many “noise sigma.”

The matched filter formally maximizes the efficiency with which the SZE survey will locate isolated clusters because it maximizes the contrast between the signal and the background noise. In a real cluster survey, however, the analysis team may wish to sacrifice efficiency somewhat if in doing so it can provide a substantial gain in the completeness of the survey. In many cases, particularly when the beam size is large, the filter in Fourier space is very narrow and filters out much of the signal, along with the noise. In addition, a narrow filter in Fourier space develops significant sidelobes in real space. When such a filter is convolved with the density spike at the location of the cluster, it enhances both the central peak and an annular region at the location of each sidelobe. In the most extreme cases, several concentric rings may appear around the central maximum that marks the location of the cluster. These rings can overlap with other rings from nearby structures in complicated ways. If these rings are misidentified as separate clusters, they negatively impact the efficiency.⁴ Thus, making the filter a little wider than the matched filter for experiments with lower resolution helps by improving the completeness significantly while it ameliorates the ringing.

2.6. Peak Finding

Even a glance at Figures 1 and 2 is enough to show that finding peaks in an SZE observation is fraught with difficulties. The peaks are often irregularly shaped, contain significant substructure, and merge with neighboring peaks. We spent considerable time trying different methods of detecting substructure, merging peaks, and imposing thresholds on either total flux or peak flux. We found that exactly which peaks passed which cuts depended on how these issues were handled but were unable to find a strategy that worked in every case. Smoothing the maps with a resolution of $1'$ or more, matched to the angular size of clusters at cosmological distances, mitigated some of the sensitivity but

⁴ Such considerations will obviously apply to any filtering technique with a compensated filter, such as, for example, a wavelet-based approach. The key parameter is the mean separation of bright sources compared with the filtering scale. If the separation is smaller than the filtering scale, the compensated filter needs to be used with caution.

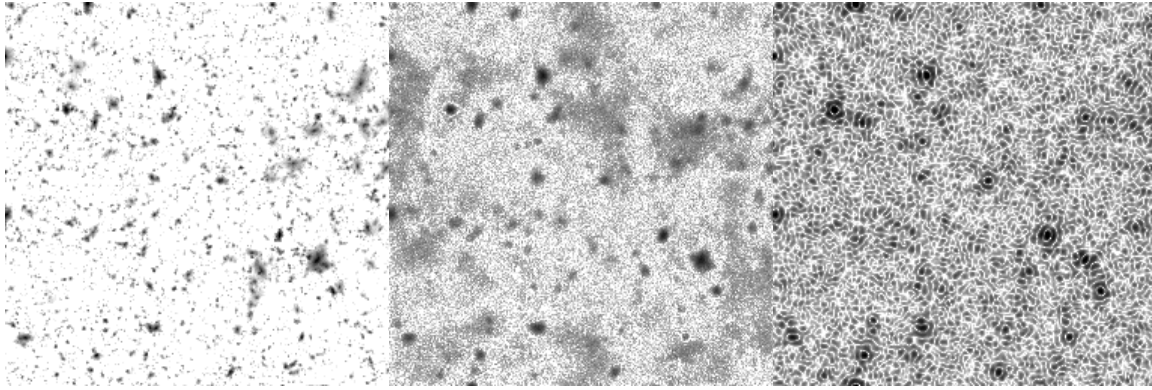


FIG. 2.—Three stages of our mock SZE survey. *Left:* Signal (*middle*) combined with the primary CMB anisotropies, smoothed with a $2'$ FWHM beam and with $5 \mu\text{K}$ per $2'$ pixel of Gaussian random “instrument” noise added (the absolute value is plotted). *Right:* Middle map filtered with the matched filter algorithm described in the text to increase the contrast of the clusters against the background (the absolute value is plotted). Each map is $3^\circ \times 3^\circ$ and contains 1024^2 pixels, rebinned to 256^2 for plotting purposes. The gray scale in each case is logarithmic, with black being 2 orders of magnitude below the peak value (*white*).

did not entirely eliminate the dependence on peak-finding properties. In particular, which peaks are found in dense environments (which may, for example, correspond to interacting halos) depends on one’s choice for peak edges and merger criteria. This is an analog of the problem we found in defining clusters in the three-dimensional data set under similar conditions.

However, we did notice that while the exact numbers were sensitive to the peak finder, the general trends we find (below) were not very sensitive. For this reason, we chose the simplest peak finder, with the fewest adjustable parameters, in order to present our results. Specifically, we used a simple algorithm, similar in nature to the one in White et al. (2002). We first record and number all the pixel locations of local maxima in the map. We search around each local maximum and include in the extended peak all pixels with a value greater than 25% of the maximum value, out to a maximum radius of 10 pixels. All peaks are extended at the same rate, so that adjacent peaks do not merge into one object. This has a tendency to split objects with significant substructure into multiple peaks, but for smoothed maps such a situation is reasonably rare. The algorithm returns a peak number (or no peak) for every pixel in the map. We have tested sensitivity to the 25% criterion for associating a pixel with a peak and find that, for the smoothed maps, completeness and efficiency are unaffected by moderate changes in this parameter. The “value” associated with a peak is the peak temperature fluctuation. Since we are smoothing on scales comparable to the total size of a peak, it makes little difference whether we choose peak temperature or total fluctuation. The fraction of peaks in the mock observation that matched at least one halo is the efficiency, and the fraction of halos that matched a peak is the completeness.

Certainly more complicated peak-finding methods could be employed; a different filter could be tried (e.g., a wavelet-based method such as described in Cayón et al. 2000 or Herranz et al. 2002, which corresponds to bandpass filtering), and more sophisticated modeling (e.g., along the lines of the CLEAN algorithm: Högbom 1974; Clark 1980) could remove some of the artifacts introduced by the filtering. Because of this, we feel that improved strategies for finding peaks in such maps is an area worthy of more attention.

3. RESULTS

We find that the number of clusters that can be recovered from the mock SZE survey is a strong function of the beam size, the level of noise, and the threshold at which we identify cluster candidates. The level of contamination of the cluster candidates also depends strongly on these quantities. In general, decreasing the beam size, decreasing the noise, and decreasing the threshold for identifying candidates in the SZE map will improve completeness at the expense of efficiency. Since efficiency is not the exact inverse of completeness, some combinations of these three parameters will yield better results than others. We also find that multifrequency information can be extremely valuable in finding clusters by removing the dominant noise source at large angular scales.

Figure 1 shows a “perfect” observation by a multifrequency instrument. The Compton- γ map has been smoothed at $1'$, but no noise or CMB has been added. The gray scale has been selected to emphasize the most prominent peaks. We have indicated the peaks corresponding to the most massive clusters in the field by solid circles and the biggest peaks in the field by dashed circles. As one can see, most of the massive clusters are easily recovered with few false positives, but there is not a 1-1 correspondence even at these high thresholds. The source of the disagreement can be traced to the large number of objects in the maps (confusion) and a scatter in the relation between the mass and the observable SZE (White et al. 2002). The sources of this scatter are threefold. First, there is a time evolution in the relation between the mass of a cluster and its temperature (eq. [1]). Since the clusters are from a large range in redshifts, this causes some scatter. Second, projection effects are nonnegligible. In fact, clusters have a tendency to form in overdense regions, often at the intersection of a beaded filamentary structure, increasing the probability of nontrivial line-of-sight projection. Finally, clusters are not spherical, and the signal strength depends on their orientation. Since the lower mass halos are intrinsically more numerous, even misidentifying a small fraction of them can negatively impact the survey efficiency.

Of course, the situation depicted in Figure 1 is highly unrealistic. To truly assess how well a survey can find

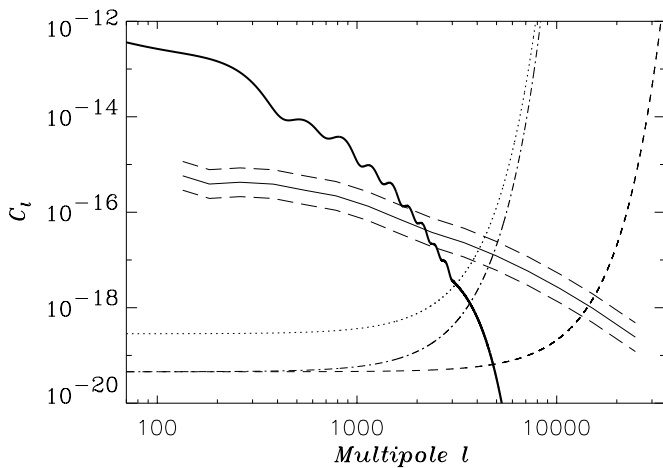


FIG. 3.—Role of sensitivity and resolution in SZE surveys. The three types of curves (from top to bottom at left of plot) are the power spectra of the primary CMB anisotropies (*thick solid line*), the SZE signal (an average of the power spectra in our ten maps, *solid and dashed lines*), and the instrument noise (*dotted, dot-dashed, and dashed lines*). The dotted curve has a $3'$ FWHM Gaussian beam with $4 \mu\text{K}$ of noise per $1'$. The dot-dashed curve has the same beam size, but $2 \mu\text{K}$ noise per $1'$. The dashed curve has a $1'$ beam with $2 \mu\text{K}$ of noise.

clusters, we need to include both astrophysical and instrument noise. The images in Figure 2 display the various stages of our mock SZE survey. The pure SZE map is shown in the left panel. The middle panel shows how the SZE signal from clusters is clouded by adding the CMB, convolving with a Gaussian beam of $1'$ angular extent, and further adding Gaussian random noise. The right panel shows the map in the middle panel after it has been filtered with the matched filter described above.

Figure 3 illustrates the role of the size of the beam and the noise level in locating clusters with an SZE survey. The three types of curves are the power spectra of the primary CMB anisotropies, the SZE signal (an average of the power spectra in our 10 maps), and the instrument noise. (In the case of multifrequency observations, the primary CMB signal could be eliminated or at least strongly suppressed.) The range of scales over which an experiment is sensitive to the SZE are those scales for which the SZE signal is not overpowered by either the CMB or the instrument noise. The dashed lines above and below the SZE power spectrum are meant to remind the reader that the normalization of the power spectrum depends nontrivially on the cosmology we have simulated, particularly on the value of σ_8 , and could change by a factor of 2 or 3 with different initial assumptions. In circumstances in which the window of SZE sensitivity is narrow, such a change profoundly affects the projected yield of an experiment. The three noise curves are plots of C_ℓ^N , which depends on the level of noise and on the beam size. For clarity, all noise levels reported are in μK per $1'$ pixel, regardless of the beam size. The dotted curve has a $3'$ Gaussian beam at FWHM with $4 \mu\text{K}$ of noise. The dot-dashed curve has the same beam size, but the level of noise has been reduced to $2 \mu\text{K}$. It is clear that reducing the level of noise has a relatively small impact on the range of scales that can be probed. In contrast, the dashed curve, which has a beam size of $1'$ with $2 \mu\text{K}$ of noise, demonstrates that decreasing the beam size has a dramatic effect on the range of sensitivity. Alternatively, using multifrequency observa-

tions to reduce the contribution of the primary anisotropies can allow one to work at lower ℓ .

3.1. Multifrequency Observations

We begin by examining maps that do not include the contribution from the CMB. Such maps could be obtained using multifrequency observations (we will not address here the methods by which component separation is done; for a recent survey of the literature see, e.g., Vielva et al. 2001 or Herranz et al. 2002) of the same field. This removes the largest source of confusion from the SZE maps. To generate these maps, we converted the Compton- γ maps to temperature fluctuation maps, smoothed them with a Gaussian filter using an fast Fourier transform, added an appropriate level of pixel (white) noise, and once again smoothed the maps. This last stage of smoothing was necessary, since our pixel scale is significantly smaller than the beam, leading to a large per-pixel noise. Smoothing the maps reduces this noise with little effect on the signal.

We find that for noise levels as low as $5 \mu\text{K}$ $1'$ per pixel, both the completeness and efficiency can be very good at high angular resolution. For thresholds above 5σ , more than 80% of the peaks correspond to rich clusters above $3 \times 10^{14} h^{-1} M_\odot$, and for beams of $1'$ FWHM, such a cut recovers 75% of the existing clusters above this mass threshold. As long as a cut of at least 4σ is applied, the efficiency is greater than 60%. For a beam smaller than $2'$ FWHM, more than half of the clusters can be recovered. However, such a low noise level may be optimistic for upcoming experiments. If we increase the noise to $10 \mu\text{K}$ per $1'$ pixel, the situation degrades. The best completeness is now around 60%, and only at low thresholds, for which the efficiencies are low. To avoid confusion, the beam also needs to be less than $1/5$ FWHM.

As a concrete example, we consider an idealization of the *Planck* satellite surveying $\sim 70\%$ of the sky. In terms of cluster finding, *Planck*'s capabilities are primarily limited by its resolution, many distant clusters subtending a much smaller angle than *Planck*'s beam size. As such, the sample found by *Planck* will be biased in that it will tend to identify the nearest clusters (see Aghanim et al. 1997 or Kay et al. 2001 for more details; see Herranz et al. 2002 for a recent study of the expected *Planck* SZE catalog). We assume that component separation has left no primary CMB signal in our SZE map. In particular, we optimistically computed the completeness and efficiency with equal parts noise from the 217 GHz (no SZE) and 353 GHz channels, added in quadrature. These channels both have an angular resolution of $5'$. Within this (overly) simplistic approximation, *Planck* finds close to half of the objects more massive than $3 \times 10^{14} h^{-1} M_\odot$, but with our simple peak finding algorithm, the efficiency is below 20%. Over 70% of the sky, this is a very large sample, useful for many studies of clusters. However, a more sophisticated cluster finding algorithm would need to be employed before this sample could be used as a cosmological probe. Improved methods for finding massive clusters in low-resolution but multifrequency data is a topic that we intend to pursue further in a future publication.

3.2. Spatial Filtering

Let us now turn to the case of single-frequency maps. In this situation, we must remove the large CMB contribution by using its spatial structure. Figures 4 and 5 are contour

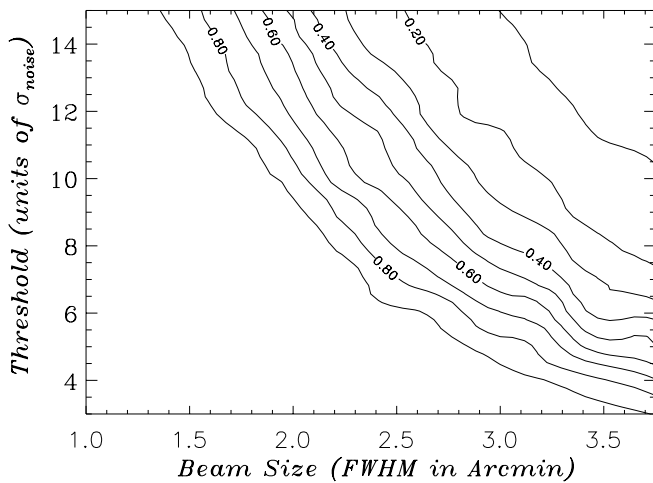


FIG. 4.—Completeness in finding halos more massive than $3 \times 10^{14} h^{-1} M_{\odot}$ in maps with noise $5 \mu\text{K}$ per $1'$ pixel with peaks selected as local maxima.

plots of the completeness and efficiency that can be achieved by a single-frequency experiment, using the optimal filter of equation (7), for various beam sizes. Again, we consider all rich clusters above $3 \times 10^{14} h^{-1} M_{\odot}$. The contours are computed at a constant noise level of $5 \mu\text{K}$ per $1'$ pixel. On the y -axis the threshold is used on the filtered plot to identify cluster candidates. The threshold indicates the statistical significance of the cluster candidate above the level of instrument noise. The 1σ value is determined by filtering the noise map without the SZE or CMB signal and computing the resulting variance. In Figure 4 the completeness improves as the resolution gets better (smaller beam); however, some percentage of the clusters are overlooked as the candidate threshold is raised. Raising the threshold is useful, however, in terms of improving the efficiency of the survey, as can be seen in Figure 5. Because all of the candidates need to be followed up for redshift information (and positive identification as a real cluster, since the contamination for some experiments can be large), efficiency is a high priority. Since the contours in Figures 4 and 5 are not completely parallel, there is not a simple trade-off between completeness and effi-

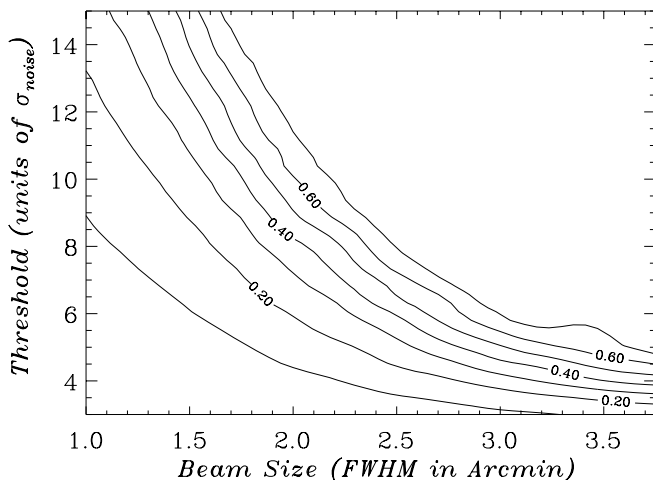


FIG. 5.—Efficiency at finding halos more massive than $3 \times 10^{14} h^{-1} M_{\odot}$ in maps with noise $5 \mu\text{K}$ per $1'$ pixel with peaks selected as local maxima.

ciency, but rather there are regions that are clearly somewhat better compromises than others.

The very low efficiencies evident in the bottom left of Figure 5 should not be read as confusion by noise in the map. There are no noise peaks of 10σ in these maps, even including the CMB! Rather, they come from lower mass halos that happen to give rise to peaks that are many sigma above the noise when the beam is small. For a $1'$ FWHM beam at $5 \mu\text{K}$, even halos with $10^{14} h^{-1} M_{\odot}$ can give rise to a greater than 5σ peak, and these outnumber the $M > 3 \times 10^{14} h^{-1} M_{\odot}$ halos 10:1. Raising the threshold even further (off the top of the plot) removes the lower mass peaks and improves efficiencies but at the expense of completeness, as in the above examples.

3.3. Nonoptimal Filter

Another degree of freedom is to change the shape of the filter instead of adjusting the threshold. As mentioned earlier, broadening the filter can improve completeness without clobbering the efficiency, because the increase in noise confusion is moderately compensated by the decrease in ringing. Broadening the filter can also decrease both the mass and distance biases that occur in SZE surveys with limited angular resolution. Figures 6 and 7 show the completeness for three different beam sizes, binned in mass and distance bins, respectively. These plots demonstrate that while high-resolution experiments are relatively unbiased, surveys with a large beam size will tend to deselect distant or less massive clusters because the angle they subtend is smaller than the resolution of the experiment. By broadening the filter (dashed lines in Figs. 6 and 7), the completeness of the sample improves, as does the bias in some cases. Decreasing the bias, or at very least quantifying it, is critical if the survey is to be used to constrain the cosmological parameters.

We find that broadening the filter on the high- ℓ side (noise side) in Fourier space is ineffective because the increase in the noise confusion is too great, completely destroying the efficiency. Instead, we have filtered less harshly on the low- ℓ portion of the mock survey, replacing the $1/C_{\ell}^{\text{CMB}}$ portion

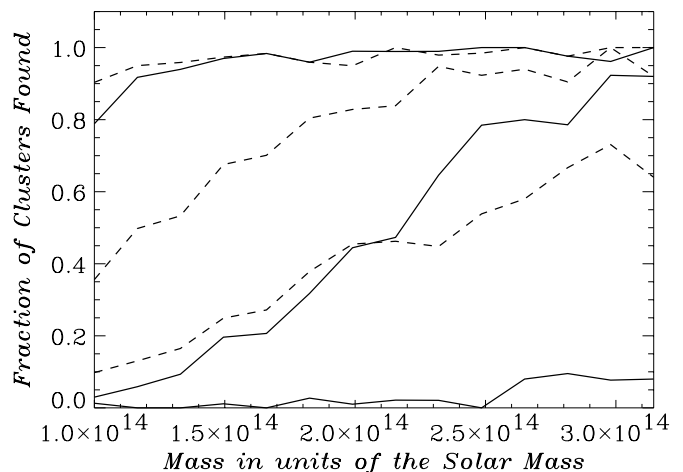


FIG. 6.—Fraction of the total number of clusters in each mass bin of width $1.75 \times 10^{13} h^{-1} M_{\odot}$ found in mock surveys of three different beam sizes: $1'$, $2.5'$, and $4'$ (top to bottom). The solid curves indicate the results when the matched filter is used; the dashed curves show the improvement in completeness when a less severe filter is employed. Slope in the curves indicates a selection bias.

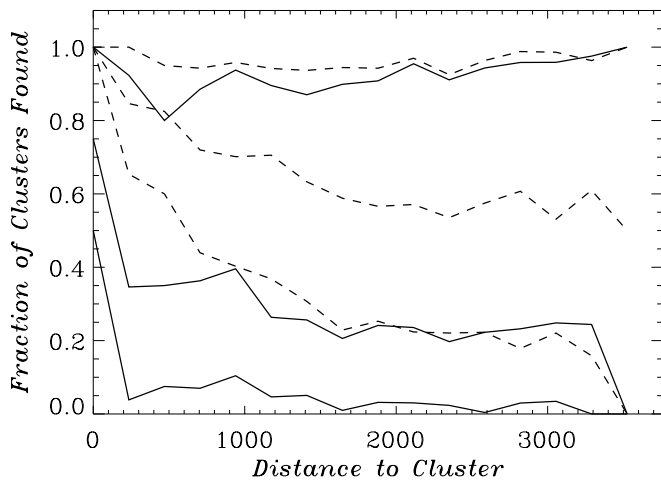


FIG. 7.—Fraction of the total number of clusters in each distance bin of width $235 h^{-1}$ Mpc found in mock surveys of three different beam sizes: $1'$, $2.5'$, and $4'$ (top to bottom). The solid curves indicate the results when the matched filter is used; the dashed curves show the improvement in completeness when a less severe filter is employed. Slope in the curves indicates a selection bias. In this cosmology, $z = 1$ is at (approximately) $2300 h^{-1}$ Mpc. The distribution of halos more massive than $3 \times 10^{14} h^{-1} M_{\odot}$ peaks at $z \sim 0.6$ or $1400 h^{-1}$ Mpc and falls by 2 orders of magnitude by $z = 2$ ($3600 h^{-1}$ Mpc).

of the filter with a much wider half Gaussian that peaks at the same value of ℓ . The improvement in the completeness is naturally accompanied by a corresponding decrease in the efficiency. The efficiencies for $4'$, $2.5'$, and $1'$ beam sizes in the matched filter case were 93%, 86%, and 52%, respectively. In the modified filters, the width of the Gaussian was chosen so that the efficiency would be approximately 45%. These widths were 1600, 2500, and 2500 ℓ values, respectively. This method could be used to satisfy any efficiency requirement lower than the efficiency of the matched filter in order to improve completeness. While we did not explicitly try it, we expect that the Mexican hat wavelet, which corresponds to a filter $x^2 e^{-x^2}$ with $x \propto \ell$, would also work well.

4. CONCLUSIONS

The SZE offers a new and potentially very powerful method for finding high-redshift clusters of galaxies. Because the amplitude of the effect is independent of the distance to the cluster, it appears to be one of the best techniques for constructing a large sample of high- z clusters.

Finding clusters with an SZE survey is, however, fraught with complications, some of which we have begun to address here using mock observations of simulated maps.

While there remains significant uncertainty in the overall level of the SZE angular power spectrum and our modeling of the effect has been somewhat crude, we already see that the requirements on frequency coverage, angular resolution, and noise are quite severe for experiments hoping to find large samples of clusters through the SZE. In single-frequency maps, the primary CMB anisotropies prove to be a large contaminant. Indeed, for experiments with angular resolutions of greater than $1'$ there is little spatial range where the SZE signal dominates.

Many important effects must be balanced when designing the experiment and analyzing the data. The angular resolution of the instrument used is of paramount importance, a key element in determining the yield of the survey. Decreasing the beam size improves the completeness and, more importantly, decreases the bias against distant and lower mass clusters. For any given resolution, however, there are adjustable parameters in the data analysis that can help reduce the bias and maximize completeness, at the moderate expense of efficiency. Efficiency is still a vital part of the survey design, however, because each cluster candidate must be followed up for positive identification and redshift information. The intrinsic contamination that occurs as a result of projection effects makes a follow-up required, even if the precise redshift is not needed. To obtain a high level of completeness with correspondingly high efficiency requires a multifrequency observation with angular resolution of $1'$ or better and noise at or below $10 \mu\text{K}$ per $1'$ pixel.

We have found that aggressive spatial filtering, to enhance the clusters against the background, can have the unwanted side effect of introducing ringing into the maps. Given the large number of sources in a typical simulated map, overlapping “rings” can produce significant false detections. Multifrequency information could help reduce some of the pitfalls inherent in a single-frequency analysis and may provide a less severe alternative than matched filtering to disentangle SZE clusters from primary CMB anisotropies. For any of these approaches, more sophisticated methods of identifying peaks in the SZE map (e.g., matched filtering) need to be investigated. Better data analysis offers the hope of increased completeness without a sacrifice in efficiency.

The authors would like to thank Nils Halverson, Erik Reese, and Chris Vale for many useful discussions on this work. The simulations used here were performed on the IBM-SP2 at the National Energy Research Scientific Computing Center. This research was supported by the NSF and NASA. M. W. was supported by a Sloan Foundation Fellowship.

REFERENCES

- Aghanim, N., da Luca, A., Bouchet, F. R., Gispert, R., & Puget, J. L. 1997, *A&A*, 325, 9
 Cayón, L., et al. 2000, *MNRAS*, 315, 757
 Clark, B. G. 1980, *A&A*, 89, 377
 Cooray, A. 2000, *Phys. Rev. D*, 62, 103506
 Cooray, A., Hu, W., & Tegmark, M. 2000, *ApJ*, 540, 1
 da Silva, A. C., Barbosa, D., Liddle, A. R., & Thomas, P. A. 2001, *MNRAS*, 326, 155
 Davis, M., Efstathiou, G., Frenk, C. S., & White, S. D. M. 1985, *ApJ*, 292, 371
 Eisenstein, D., & Hu, W. 1999, *ApJ*, 511, 5
 Finoguenov, A., Reiprich, T. H., & Bohringer, H. 2001, *A&A*, 368, 749
 Haehnelt, M., & Tegmark, M. 1996, *MNRAS*, 279, 545
 Herranz, D., et al. 2002, *MNRAS*, 336, 1057
 Högbom, J. 1974, *A&AS*, 15, 417
 Holder, G., & Carlstrom, J. 2001, *ApJ*, 558, 515
 Kay, S. T., Liddle, A. R., & Thomas, P. 2001, *MNRAS*, 325, 835
 Kochanek, C. S., White, M., Huchra, J., Macri, L., Jarret, T. H., Schneider, S. E., & Mader, J. 2003, *ApJ*, 585, 161
 Komatsu, E., & Kitayama, T. 1999, *ApJ*, 526, L1
 Komatsu, E., & Seljak, U. 2002, *MNRAS*, 336, 1256
 Mason, B. S., et al. 2002, *ApJ*, submitted (astro-ph/0205384)
 Molnar, S. M., & Birkinshaw, M. 2000, *ApJ*, 537, 542
 Seljak, U., & Zaldarriaga, M. 1996, *ApJ*, 469, 437
 Tegmark, M., & de Oliveira-Costa, A. 1998, *ApJ*, 500, L83
 Tegmark, M., & Efstathiou, G. 1996, *MNRAS*, 281, 1297
 Vielva, P., et al. 2001, *MNRAS*, 328, 1
 White, M. 2002, *ApJS*, 143, 241
 White, M., Hernquist, L., & Springel, V. 2002, *ApJ*, 579, 16
 White, M., & Kochanek, C. 2002, *ApJ*, 574, 24
 White, M., van Waerbeke, L., & Mackey, J. 2002, *ApJ*, 575, 640